Higly Luminescent Aceno[6]helicenones by Intramolecular Radical Cyclization

Ludmilla Sturm, Marzena Banasiewicz, Irena Deperasinska, Boleslaw Kozankiewicz, Olaf Morawski, Pierre Dechambenoit, Harald Bock, Yuuya Nagata, Ludovic Salvagnac, Isabelle Séguy, et al.

Highly Luminescent Aceno[6]helicenones by Intramolecular Radical Cyclization

Ludmilla Sturm,[a] Marzena Banasiewicz, [b] Irena Deperasinska, [b] Boleslaw Kozankiewicz, [b] Olaf Morawski, [b] Pierre Dechambenoit, [a] Harald Bock, [a] Yuuya Nagata, [c] Ludovic Salvagnac, [d] Isabelle Séguy, [d] Michal Šámal*[e] and Andrej Jančařík*[a]

[a] Dr., L. Sturm, Dr. P. Dechambenoit, Dr. H. Bock, Dr. A. Jancarik
Centre de Recherche Paul Pascal, CRPP, UMR 5031
Université de Bordeaux, CNRS
33600 Pessac, France.
E-mail: Andrej.jancarik@crpp.cnrs.fr

[b] Dr. M. Banasiewicz, Prof. I. Deperasinska, Prof. B. Kozankiewicz, Dr. O. Morawski
Institute of Physics
Polish Academy of Sciences
Al. Lotników 32/46, 02-668 Warsaw, Poland

[c] Dr. Y. Nagata
Japan Institute for Chemical Reaction Design and Discovery (WPI-ICReDD)
Hokkaido University,
Sapporo, Hokkaido 001-0021, Japan

[d] Dr. I. Seguy
LAAS-CNRS
Université de Toulouse, UPS,
31031 Toulouse, France

[e] Dr. M. Šámal
Institute of Organic Chemistry and Biochemistry of the Czech Academy of Sciences,
166 10 Prague 6, Czech Republic
E-mail: michal.samal@uochb.cas.cz

Supporting information for this article is given via a link at the end of the document.

Abstract: Helicenes and helicenoid structures are promising candidates for future applications exploiting circularly polarized light. Ideal candidates should possess near-quantitative photoluminescence quantum yield, a high luminescence dissymmetry factor and an adjustable HOMO-LUMO gap. However, carbo[n]helicenes are poorly luminescent compounds and they absorb light mainly in the ultraviolet region. Here we show that the incorporation of a carbonyl group into helical scaffold significantly improves the fluorescence quantum yield and shifts the absorption to visible region. Although the carbonyl group is commonly considered as detrimental to efficient emission, fluorescence quantum yields up to $\Phi = 0.43$ were recorded. A straightforward synthetic approach to a highly luminescent tetraceno[6]helicenone and an aza analogue has been developed. The key step is a radical cyclization which is achieving dehydrative π-extension. The aza-analogue was incorporated as an emitter in organic light emitting diodes (OLEDs) and showed good performance.

Introduction

Carbo[n]helicenes are a class of nonplanar inherently chiral aromatic hydrocarbons that have attractive physicochemical properties such as 3D electron delocalization, strong chiroptical properties and much better solubility than planar aromatic systems. Thus, helicenes and/or helicenoid structures are intensively studied as ligands in enantioselective catalysis, active components in organic electronics and photonics or as building blocks in supramolecular chemistry.[1–3] Due to their robust intrinsic chirality, helicenes are good candidates for applications that require circularly polarized light such as CP-OLEDs/OLETs, three-dimensional (3D) displays, and chiroptical switches.[1,4] Two key parameters, the dissymmetry factor g_{lum} and the photoluminescent quantum yield (Φ), have to be optimized to render the compounds attractive for wider use. However, they are usually only weakly luminescent ($\Phi_F \leq 0.04$) and show only moderate g_{lum} values ($g_{lum} < 10^{-2}$). Therefore, many efforts have been invested to tackle this issue.[5,6] Recently,[7] we have shown that a carbonyl group at the periphery of the helical backbone shifts the absorption to the visible region and improves considerably the fluorescence quantum yield.

The carbonyl group has been incorporated into the helicene to form an acenohelicene (Family **AH-I,** Figure 1) with a phenalenone central part. Connection in this fashion, where the helicene wing is condensed into a peri-position of an acene, can provide three different isomers which differ only in the position of

the carbonyl group (Families **AH-I**, **AH-II** and **AH-III**). The family **AH-I** is composed of an untouched helicene resonance structure and the carbonyl is attached at the acene-only ring of the phenalene centre. The **AH-III** family retains an acene resonance structure, with the carbonyl at a solely helicenic ring. In the present contribution we concentrate on the family **AH-II**, where the carbonyl group is part of both, the acene and the helicene substructures. We show that the position of the carbonyl has a considerable effect on the physicochemical properties in the aceno[n]helicenones.

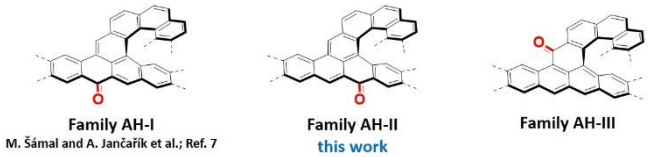

Figure 1. Three different isoelectronic acenohelicenones which differ only in the position of the carbonyl group.

Results and Discussion

Synthesis of substituted helicenes longer than [5]helicene is a challenging task that requires often multistep pathways that afford the final helicene in very small yields. In our approach the tetraceno[6]helicenone **AH-II-6** and its aza-analogue **aza-AH-II-6** were prepared in only two synthetic steps (Figure 2a) with good yields starting from commercially available 5,12-naphthacenequinone **1**. The synthesis began by addition of the in-situ generated aryl-lithium salt of **2** to the quinone **1**. Due to steric reasons, only mono-addition was observed.

No addition was observed in traditional solvents such as diethyl ether or tetrahydrofuran, as the reactivity of the organolithium compounds is highly dependent on the solvent. In coordinating solvents like ethers, the organolithium salts exist in the form of aggregates or clathrates which reduce their reactivity. When we conducted the addition in toluene, in which they exist as monomeric species, the addition occurred smoothly and only a single product was formed. The formed hydroxy-derivative **3** is thereafter, without isolation, transformed into the helicenic target **AH-II-6** or **aza-AH-II-6** within only a few minutes, presumably following our proposed mechanism (Figure 2b). After generation of the alkoxide derivative **3**, this intermediate is poured into a highly acidic and poorly reducing solution. Then, the transformation to the final helicene begins by protonation of the lithium alkoxide group (ROLi) and cleavage of the acetal group leading to **I**. Then protonation of the OH group generates the oxonium ion **II**, and subsequent elimination of water generates the triaryl cation **III**.

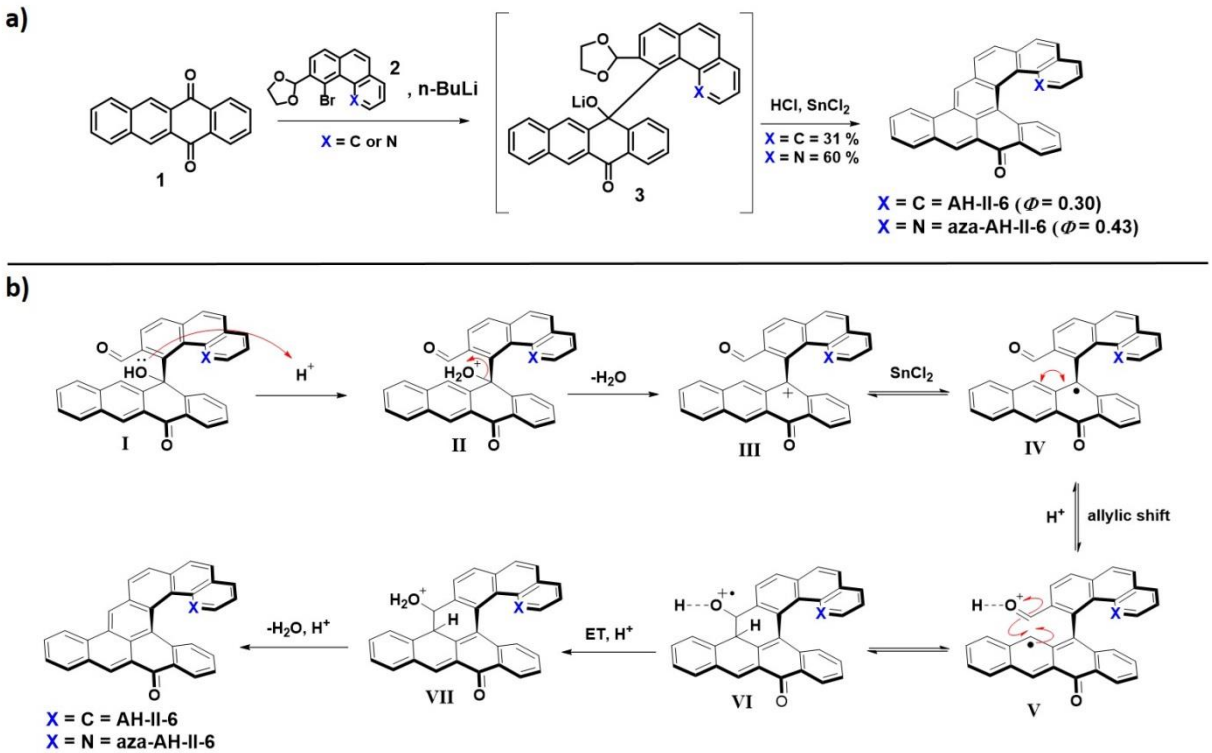

Figure 2. a) Synthesis of **AH-II-6** and its aza-analogue **aza-AH-II-6** b) Proposed mechanism of the final radical cyclization

This cation is reduced with $SnCl_2$ (which is not strong enough to reduce the carbonyl groups) to the allyl-type radical **IV** and its resonance structure **V**. The intramolecular addition of the radical to the aldehyde group provides alkoxy radical cation **VI**, which is intercepted via a subsequent electron transfer. The protonation of the OH group yields **VII**, and subsequent elimination of water completes the formation of the final helicene **AH-II-6** or **aza-AH-II-6**. Optimization studies revealed that at least two equivalents of $SnCl_2$ are necessary to smoothly convert the intermediate **3**. A lower amount of $SnCl_2$ results in a substantial decrease in the yield of the final helicenes. No product is observed in the absence of $SnCl_2$, which suggests that the formation of the allylic radical (**III** → **IV**) is a crucial step for the cyclization. In the case of **aza-AH-II-6**, the product precipitated out of the solution as a salt which can be reason for its higher yield. The reaction pathway was supported by DFT calculations at (U)ωB97X-D/Def2SVP level (see SI, page S35). The calculated energy profile diagram shows that the highest point is the transition **V** → **VI** with a barrier of only 53.1 kJ/mol. This validates that the reaction can proceed effectively at room temperature. Among several tested solvents, only dichloromethane provided satisfactory results (see SI, page S10). This radical cyclization is similar to the dehydrative π-extension (DPEX) reported by K. Amsharov et al.[8,9] Currently, the scope and limits of the radical cyclization is under examination.

Photophysical and electrochemical properties of AH-II-6 and aza-AH-II-6

AH-II-6 and **aza-AH-II-6** both are red solids with absorption onsets in nonpolar hexane (10^{-5} M) λ_{onset} = 509 nm and λ_{onset} = 498 nm (Figure 3a). When compared to isoelectronic **AH-I-6** (λ_{onset} = 479 nm) that differs only in the position of the carbonyl group, the absorption onset is shifted by 30 nm or 19 nm (1230 cm^{-1} and 796 cm^{-1}). The lowest-energy absorption bands arise from allowed π→π* transitions with high oscillator strengths (f = 0.217 for **AH-II-6**; f = 0.262 for **aza- AH-II-6**) and correspond mainly to $S_0 \rightarrow S_1$ transitions. The emission spectra in nonpolar hexane show two emission peaks with two maxima located at 516 nm and 540 nm for **AH-II-6** and 507 nm and 529 nm for **aza-AH-II-6**. We suppose that the emission with lower frequency originates from π-π stacked dimers, as significant amounts of the dimers were observed by mass spectrometry. The emission maxima of **AH-II-6** (λ_{max} = 578 nm) and **aza-AH-II-6** (λ_{max} = 561 nm) in polar dichloromethane (DCM) are located in the yellow region, whereas the maximum of **AH-I-6** (λ_{max} = 513 nm) in DCM is located in the green region (Figure 3c). The much larger bathrochromic shift in polar acetonitrile compared to non-polar hexane (33 nm → 100 nm; 1330 cm^{-1} → 3511 cm^{-1} for **AH-II-6**; 36 nm → 90 nm; 1514 cm^{-1} → 3251 cm^{-1} for **aza-AH-II-6**) indicates that the lowest excited states (S_1) have charge-transfer (CT) character with a large dipole moment. Here the carbonyl group behaves as an acceptor unit owing to its strong electron-withdrawing effect, and the electron-rich helicene wing functions as a donor. This can be seen from the electronic distributions in the HOMO and the LUMO (Figure 3f and S29).

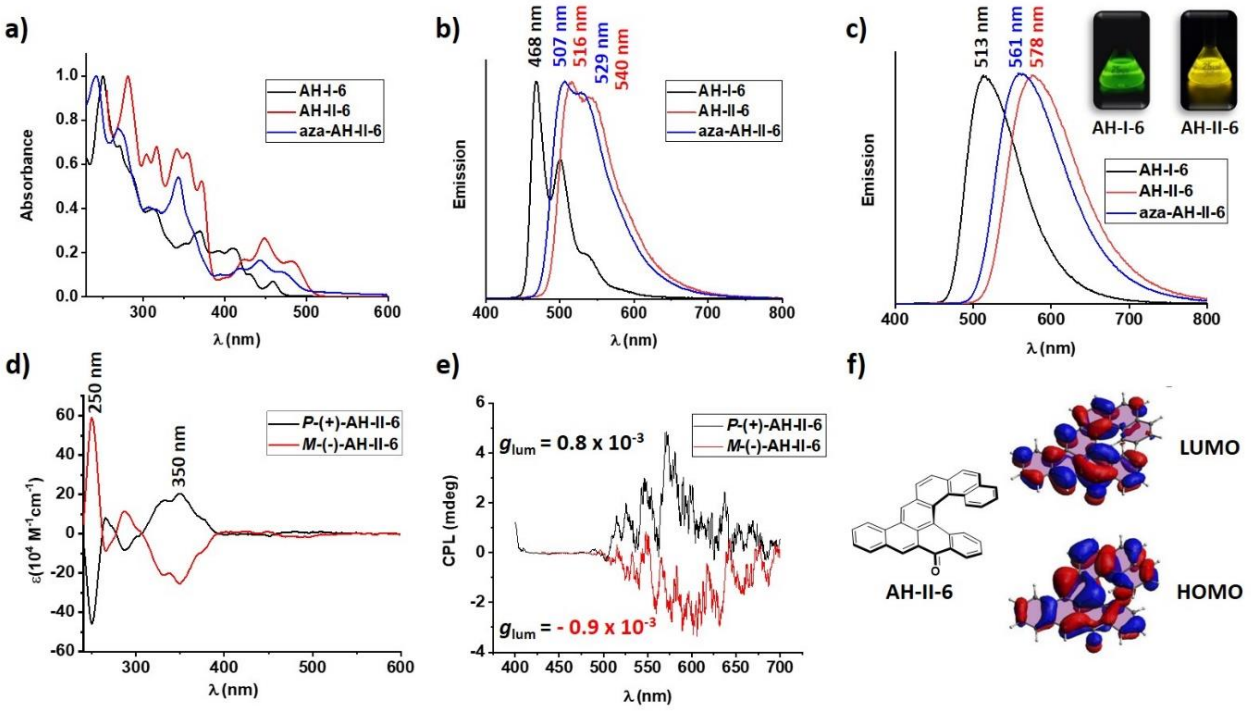

Figure 3. a) Normalized absorption spectra of **AH-I-6**, **AH-II-6** and **aza-AH-II-6** in hexane b) Normalized emission spectra of **AH-I-6**, **AH-II-6** and **aza-AH-II-6** in hexane c) Normalized emission spectra of **AH-I-6**, **AH-II-6** and **aza-AH-II-6** in DCM d) Circular dichroism spectra of **AH-II-6** in DCM e) CPL spectra of (*P*) and (*M*) enantiomers of **AH-II-6** in DCM, (c ≈ 1 x 10^{-5} M) f) Electronic configuration of **AH-II-6**.

Helicene	$\lambda_{(max)}$ [nm] DCM	$\lambda_{(em)}$ [a] [nm] DCM	g_{lum} [b] (10^{-3}) DCM	$[\alpha]_D^{20}$ DCM	B_{CPL} [c]	Φ_{PL} [d] (%) hexane/DCM/ACN	τ_{fl} [ns] hexane/DCM/ACN	k_r [e] [10^7 s^{-1}] hexane/DCM/ACN	k_{nr} [f] [10^7 s^{-1}] Hexane/DCM/ACN	E_{HOMO} [g] [eV]	E_{LUMO} [h] [eV]	$E_{(0,0)}$ [i] [eV] DCM (hexane)	$E_{(0,0)}$ [j] [eV]
AH-I	467	513	+1.7 -1.5	+2147 -2167	6.6	3.6/12.5/11.4	2.34/4.0/4.25	1.5/3.1/2.7	41.2/21.9/20.8	-6.05	-3.21	2.68 (2.84)	2.59
AH-II	494	578	+0.8 -0.9	+2031 -2098	7.8	5.3/33/32	1.98/15.63/19.2	2.7/2.1/1.7	47.8/4.3/3.5	-5.55	-3.24	2.31 (2.43)	2.27
aza-AH-II	483	561	-	-	-	4/43/40	1.06/12.2/15.3	3.8/3.5/2.6	90.6/4.6/3.9	-5.66	-3.28	2.38 (2.49)	2.32

Table 1. Comparison of electronic and photophysical properties of **AH-I**, **AH-II** and **aza-AH-II**. a) Excitation at 330 nm b) Measured in DCM ($c \approx 1 \times 10^{-5}$ M) c) Brightness calculated as $B_{CPL} = \epsilon_{max} \times \Phi_{PL} \times |g_{lum}|/2$ e) Measured at room temperature ($c \approx 1 \times 10^{-6}$ M) e) Radiative rate constant calculated as $k_r = \Phi_{PL}/\tau_{fl}$ f) Nonradiative decay rate constant calculated as $\Phi_{PL} = k_r/(k_r+k_{nr})$ g) Calculated as $E_{HOMO} = E_{LUMO} - E(0,0)$ h) Calculated using the equation E_{LUMO} = -[E'red/onset + 4.8] referenced against Fc/Fc^{+}[10] i) Optical gap determined from the intersection of the absorption and emission curves and using equation $E_g = hc/\lambda$ j) Theoretical HOMO-LUMO gap calculated by TDDFT M06/6-31G(d,p).

Although the HOMO and the LUMO are delocalized over the whole molecule, the main density of the HOMO is located on the helicene wing and the main density of the LUMO is distributed over the carbonyl-acene part. This shift of electron distribution from the HOMO to the LUMO is responsible for the CT character. However, this cannot be treated as a pure CT transition since the frontier orbitals are not fully separated. Thus, a hybrid of CT and local π→π* transitions is present.[11] The Φ_F of **AH-II-6** and **aza-AH-II-6** increases several times when passing from nonpolar hexane to polar acetonitrile (Φ_F of **AH-II-6** 0.05 → 0.32 and Φ_F of **aza-AH-II-6** 0.04 → 0.40, see Table 1). It should be noticed that the fluorescence quantum yields Φ_F for both, **AH-II-6** and **aza-AH-II-6** compounds, are significantly higher than that for the isoelectronic structure **AH-I-6** (Φ_F of **AH-I-6** in hexane → acetonitrile 0.04 → 0.11). Higher fluorescence quantum yield of **AH-II-6** and of its aza-analogue is probably related to less efficient intersystem crossing than in the case of **AH-I**. According to our quantum-chemistry calculations (see SI, page S33) in case of **AH-II** only one triplet state, T_2, is close in energy to the singlet S_1 state, and this state can contribute to the intersystem crossing to the triplet manifold. Such presumption is confirmed by the strong dependence on the solvent polarity. The fluorescence lifetimes (τ_{fl}) of both studied compounds, **AH-II-6** and **aza-AH-II-6**, observed in nonpolar hexane (**AH-II-6** τ_{fl} = 1.98 ns and **aza-AH-II-6** τ_{fl} = 1.06 ns) are much shorter than the corresponding values observed in highly polar acetonitrile (**AH-II-6** τ_{fl} = 19.2 ns and **aza-AH-II-6** τ_{fl} = 15.3 ns). Fluorescence lifetimes of considered compounds in nonpolar hexane are comparable with the lifetimes observed for acenohelicenes **AH-I** (2-4 ns) and shorter than those for the corresponding carbo[n]helicenes (10-15 ns)[12]. The above observations press us to propose that in nonpolar solvents the triplet T_2 state of **AH-II** is located at lower energy than the singlet S_1, thus making possible the intersystem crossing channel $S_1 \rightarrow T_2 \rightarrow T_1$, whereas in polar solvents the S_1 state is shifted below the T_2, thus blocking this relaxation channel ($S_1 \rightarrow T_2$ would require thermal activation). Lack of phosphorescence of both the **AH-II-6** and **aza-AH-II-6** from the T_1 state is not surprising. The high energy difference of $E_{S1\text{-}T1}$ (0.7 eV for **AH-II-6** and 0.72 eV for **aza-AH-II-6**) $E_{T2\text{-}T1}$ (0.73 eV for **AH-II-6** and 0.77 eV for **aza-AH-II-6**) renders the T_1 state hard to access and in addition, we should take into account that this state is located some 1.5 eV above the ground state and may relax non-radiatively.

Cyclic voltammetry (CV) measurements were performed in acetonitrile to determine the redox properties of **AH-II-6** and **aza-AH-II-6**. **AH-II-6** exhibits three and **aza-AH-II-6** two reversible reduction processes, whereas neither shows any oxidation wave below +1.0 V (vs Fc/Fc+), suggesting a poor electron donating ability of the helicene wing (see SI, page S23-S26). In comparison, the isoelectronic **AH-I-6** exhibits two reduction processes, of which the second one is irreversible. From the onset of the reduction wave, the LUMO energy levels of **AH-II-6** (E_{LUMO} = - 3.24 eV) and **aza-AH-II-6** (E_{LUMO} = - 3.28 eV) were calculated. These values are lower than the LUMO of **AH-I-6** (E_{LUMO} = - 3.21 eV). The HOMO energy levels were calculated from the absorption onset wavelength (**AH-II-6**, E_{HOMO} = - 5.55 eV; for **aza-AH-II-6** E_{HOMO} = - 5.66 eV).

The poor solubility of **aza-AH-II-6** did not allow us to resolve its enantiomers, and we could separate only the enantiomers of **AH-II-6** by HPLC on a chiral stationary phase column (IE). The absolute configurations were assigned by circular dichroism (CD) spectroscopy with the aid of TD-DFT calculations (see Si, page S27). The first-eluting fraction was assigned as the *P*-(+) and the second one as *M*-(-) enantiomer. The enantiomers give CD spectra with strong opposite Cotton effects (Figure 3d). The highest dissymmetry factor (***P*-AH-II-6**: $g_{abs} = \pm 3.3 \times 10^{-3}$ was found for the band with maximum at 350 nm). The very broad band at 458 – 546 nm with $g_{abs} = \pm 0.5 \times 10^{-3}$ (***P*-AH-II-6**), is assigned to $S_0 \rightarrow S_{1,2}$ transitions. The CPL spectra (Figure 3e) have moderate $g_{lum} = 0.8/-0.9 \times 10^{-3}$, and the sign of the CPL matches that of the CD. The g_{lum} is slightly lower than the g_{lum} of **AH-I-6** ($g_{lum} = 1.7/-1.5 \times 10^{-3}$).

The negligible gap between S_1 and T_2 ($E_{S1\text{-}T2}$ = -27 meV for **AH-II-6** and $E_{S1\text{-}T2}$ = - 44 meV for **aza-AH-II-6**) plus high spin orbit coupling (SOC = 0.236 cm^{-1} for **AH-II-6** and 0.255 cm^{-1}) and the high energy difference of $E_{T2\text{-}T1}$ (0.73 eV for **AH-II-6** and 0.77 eV for **aza-AH-II-6**) are good prerequisites of harvesting high-lying triplet states to singlet states during the electroluminescent processes.[13,14] This motivates us to evaluate the electroluminescence (EL) of our compounds. We fabricated the vacuum deposited OLEDs.

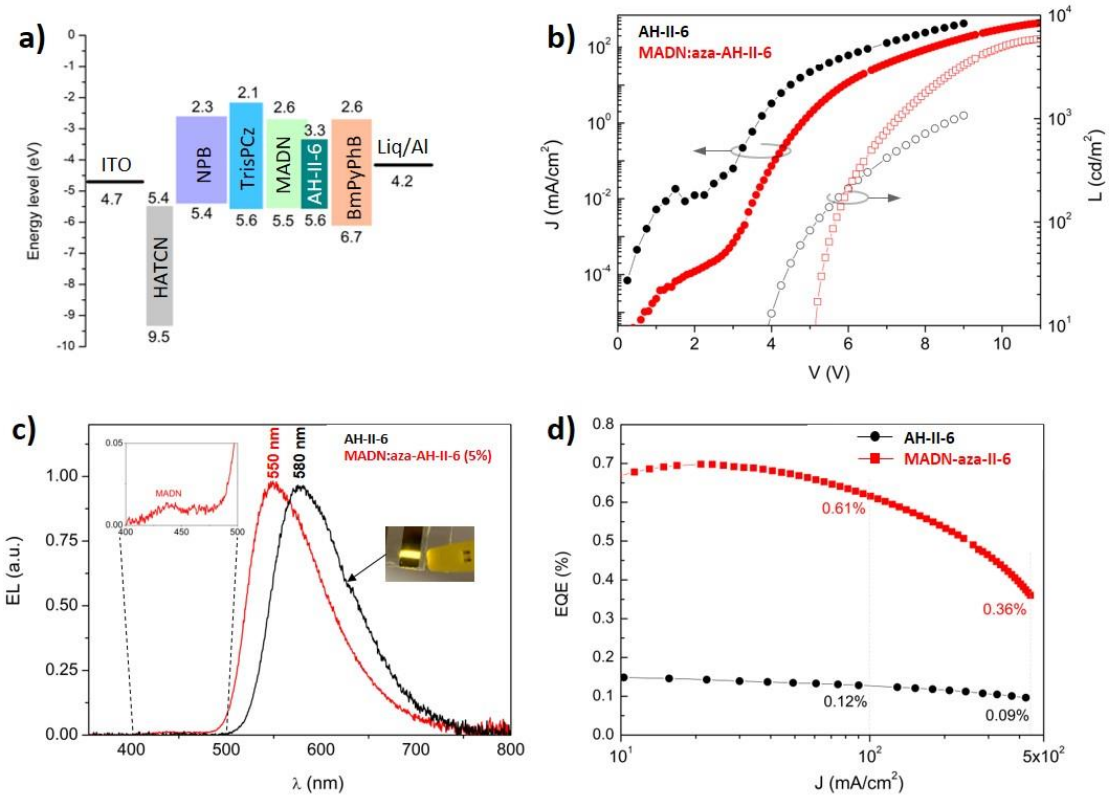

Figure 4: a) Schematic energy-level diagram of the OLEDs D1 and D2 . b) current-density-luminance-voltage (J-L-V) characteristics, c) normalized EL spectra measured at 7V, and d) EQE-J plots for the **aza-AH-II-6** (black) and MADN:**aza-AH-II-6** (red) EML based devices.

Table 2. Summary of EL performances for devices based on **aza-AH-II-6** and MADN:**aza-AH-II-6** (95:5) as EML

Device	V_{on} (V)	L_{max} (cd/m^2)	EQE_{max} (%)	EQE $_{@\ 1000\ cd/m^2}$ (%)	CE_{max} (cd/A)	PE_{max} (Lm/W)	λ_{peak} (nm)	FWHM (nm)
D1	3.7	1072	0.15	0.1	0.25	0.09	580	103
D2	5	5887	0.7	0.64	1.35	0.39	550	93

V_{on} = turn-on voltage at ~7 cd/m^2, L_{max}= maximum luminance, EQE_{max}= maximum external quantum efficiency, CE_{max} = maximum luminance efficiency, PE_{max} = maximum power efficiency, λ_{peak}= peak of emission in EL spectrum

The OLED stack (Figure 4a) was: ITO / HATCN (5nm) / NPB (40 nm) / Tris-PCz (15 nm) / EML (20 nm) / BmPyPhB (40 nm)/ Liq (1.5 nm)/Al (100nm) where 1,4,5,8,9,11-hexaazatriphenylene hexacarbonitrile (HATCN) was used as the hole injection layer, 4,4'-N,N'-bis[N-(1-naphthyl)-N-phenylamino] biphenyl (NPB) as the hole transport layer, 9-phenyl-3,6-bis(9-phenyl-9Hcarbazol-3-yl)-9H-carbazole (Tris-PCz) as electron blocking layer (EBL), 1,3-bis(3,5-dipyrid-3-ylphenyl)benzene (BmPyPhB) as electron transport layer (ETL), and 8-hydroxyquinolinolato-lithium (Liq) as electron injection layer (EIL). Two different emitting layers (EML) were prepared with either pristine **aza-AH-II-6** (OLED stack D1) or MADN:**aza-AH-II-6** (OLED stack D2) obtained by the co-evaporation of MADN and **aza-AH-II-6** in a 19:1 ratio. The current density-voltage-luminance (J-L-V) characteristics and the EQE versus current density/luminance are shown in Figure 4b and the device parameters are summarized in Table 2. Both OLEDs exhibited broad and structureless EL spectra centered at 580 nm and 550 nm with FWHM of 90-100 nm (Figure 4c) and maximum EQE of 0.15% and 0.64% for pristine and MADN:**aza-AH-II-6** EML. For D1 the EL spectrum is similar to the PL obtained from vacuum-deposited thin films of **aza-AH-II-6** (see SI, S34). The modest EQE value obtained of D1 is probably caused by aggregation-caused quenching (ACQ) in the thin film of **aza-AH-II-6 (**the Φ_F of **aza-AH-II-6** in solid state is only 4.7%).[15] D2 with a MADN:**aza-AH-II-6** host-guest layer as EML was made to overcome this issue. In the electroluminescence spectrum of D2, the emission peak is shifted by 30 nm towards the blue and a secondary peak due to the MADN electroluminescence is observed in the blue region (λmax = 450 nm). These features indicate incomplete energy transfer between the MADN and **aza-AH-II-6** which limited the efficiency of this device. The two OLED configurations display very low efficiency roll-off with a EQE greater than half of its maximum value for current density up to 500 mA/cm^2 and a critical luminance L90%[16] of 1781 cd/m^2 for

D2 (Figure 4d and SI page S34). The low EQE suggests that there is no obvious “hot exciton” channel which could harvest the non-radiative triplet excitons. This is probably due to the absence of hybridized local and charge-transfer excited state (HLCT).[17] This indicates that if HLCT is not present, the minimal gap between singlet and triplet states and high SOC are not enough to guarantee the reverse intersystem crossing (ISC).

Conclusion

In summary, we have developed a highly luminescent tetraceno[6]helicenone and an aza-analogue obtained by using a new synthetic approach. The synthetic key step is a dehydrative π-extension (DEPX) by radical cyclization. We have shown that the carbonyl group, generally considered as detrimental to the emission, greatly enhances the photoluminescence quantum yield. Furthermore, the installation of the carbonyl group shifts the absorption and emission spectra into the visible region. We analyzed the structural, photophysical and chiroptical properties of both helicenones using several experimental techniques and the results were supported by the TD-DFT calculations. The aza-derivative was tested as an emitting layer in the OLED structure.

Supporting Information

The authors have cited additional references within the Supporting Information.[18–23]

Acknowledgements

Calculations were performed at the Interdisciplinary Center for Mathematical and Computational Modeling (ICM) University of Warsaw under computational allocation G91-1402. The authors thank Reiko Oda for using her CD and CPL facility, Ivo Starý and Irena Stará for using their chiral HPLC facility. Mathieu Rouzieres is thanked for his drawings. This work was supported by the University of Bordeaux, the Région Nouvelle Aquitaine, Quantum Matter Bordeaux (QMBx) and the Centre National de la Recherche Scientifique (CNRS). This work was supported by the Czech Science Foundation (Reg. No. 20-23566S) and the Institute of Organic Chemistry and Biochemistry, Czech Academy of Sciences (RVO: 61388963). This work was partly supported by JSPS KAKENHI grant numbers JP21H01924 and JP23H03810, and JST via the ERATO grant JPMJER1903 and the CREST grant JPMJCR2001. The computation was partly performed using Research Center for Computational Science, Okazaki, Japan (Project: 23-IMS-C119). Support was also provided by the Institute for Chemical Reaction Design and Discovery (ICReDD), established by the World Premier International Research Initiative (WPI), MEXT, Japan.

Keywords: helicenes • acenes • spectroscopy • circularly polarized light • OLEDs •

[1] C.-F. Chen, Y. Shen, *Helicene Chemistry*, Springer Berlin Heidelberg, Berlin, Heidelberg, **2017**.
[2] J. Crassous, I. G. Stará, I. Starý, Eds. *Helicenes: Synthesis, Properties and Applications*, Wiley, **2022**.
[3] D. Sakamoto, I. Gay Sánchez, J. Rybáček, J. Vacek, L. Bednárová, M. Pazderková, R. Pohl, I. Císařová, I. G. Stará, I. Starý, *ACS Catal.* **2022**, *12*, 10793–10800.
[4] P. Ravat, T. Šolomek, M. Juríček, *ChemPhotoChem* **2019**, *3*, 180–186.
[5] J. Crassous, in *Circularly Polarized Luminescence of Isolated Small Organic Molecules* (Ed.: T. Mori), Springer Singapore, Singapore, **2020**, pp. 53–97.
[6] T. Mori, Ed. , *Circularly Polarized Luminescence of Isolated Small Organic Molecules*, Springer Singapore, Singapore, **2020**.
[7] M. Šámal, L. Sturm, M. Banasiewicz, I. Deperasinska, B. Kozankiewicz, O. Morawski, Y. Nagata, P. Dechambenoit, H. Bock, A. Rossel, M. Buděšínský, A. Boudier, A. Jančařík, *Chem. Sci.* **2024**, *15*, 9842–9850.
[8] D. Lungerich, O. Papaianina, M. Feofanov, J. Liu, M. Devarajulu, S. I. Troyanov, S. Maier, K. Amsharov, *Nat. Commun.* **2018**, *9*, 4756.
[9] M. Feofanov, V. Akhmetov, K. Amsharov, *Chem. Eur. J.* **2021**, *27*, 17268–17268.
[10] R. M. G. Rajapakse, D. L. Watkins, T. A. Ranathunge, A. U. Malikaramage, H. M. N. P. Gunarathna, L. Sandakelum, S. Wylie, P. G. P. R. Abewardana, M. G. S. A. M. E. W. D. D. K. Egodawele, W. H. M. R. N. K. Herath, S. V. Bandara, D. R. Strongin, N. H. Attanayake, D. Velauthapillai, B. R. Horrocks, *RSC Adv.* **2022**, *12*, 12089–12115.
[11] W. Li, Y. Pan, R. Xiao, Q. Peng, S. Zhang, D. Ma, F. Li, F. Shen, Y. Wang, B. Yang, Y. Ma, *Adv. Funct. Mater.* **2014**, *24*, 1609–1614.
[12] E. Vander Donckt, J. Nasielski, J. R. Greenleaf, J. B. Birks, *Chemical Physics Letters* **1968**, *2*, 409–410.
[13] Y. Xu, P. Xu, D. Hu, Y. Ma, *Chem. Soc. Rev.* **2021**, *50*, 1030–1069.
[14] P. Jin, Y. Han, F. Tian, L. Wang, X. Zhao, C. Zhang, J. Xiao, *Chem. Eur. J.* **2020**, *26*, 3113–3118.
[15] Y. Huang, J. Xing, Q. Gong, L.-C. Chen, G. Liu, C. Yao, Z. Wang, H.-L. Zhang, Z. Chen, Q. Zhang, *Nat. Commun.* **2019**, *10*, 169.
[16] C. Murawski, K. Leo, M. C. Gather, *Adv. Mater.* **2013**, *25*, 6801–6827.
[17] W. Li, Y. Pan, L. Yao, H. Liu, S. Zhang, C. Wang, F. Shen, P. Lu, B. Yang, Y. Ma, *Adv. Optical Mater.* **2014**, *2*, 892–901.
[18] E. Kaneko, Y. Matsumoto, K. Kamikawa, *Chem. Eur. J.* **2013**, *19*, 11837–11841.
[19] N. Takenaka, R. S. Sarangthem, B. Captain, *Angew. Chem. Int. Ed.* **2008**, *47*, 9708–9710.
[20] B. Kozankiewicz, *Chemical Physics Letters* **1990**, *173*, 417–420.
[21] V. Barone, J. Bloino, M. Biczysko, F. Santoro, *J. Chem. Theory Comput.* **2009**, *5*, 540–554.
[22] S. Maeda, Y. Harabuchi, *WIREs Comput Mol Sci* **2021**, *11*, e1538.
[23] Frisch, M. J.; Trucks, G. W.; Schlegel, H. B.; Scuseria, G. E.;Robb, M. A.; Cheeseman, J. R.; Scalmani, G.; Barone, V.; Petersson,G. A.; Nakatsuji, H.; Li, X.; Caricato, M.; Marenich, A. V.; Bloino, J.;Janesko, B. G.; Gomperts, R.; Mennucci, B.; Hratchian, H. P.; Ortiz, J.V.; Izmaylov, A. F.; Sonnenberg, J. L.; Williams; Ding, F.; Lipparini,F.; Egidi, F.; Goings, J.; Peng, B.; Petrone, A.; Henderson, T.;Ranasinghe, D.; Zakrzewski, V. G.; Gao, J.; Rega, N.; Zheng, G.;Liang, W.; Hada, M.; Ehara, M.; Toyota, K.; Fukuda, R.; Hasegawa, J.;Ishida, M.; Nakajima, T.; Honda, Y.; Kitao, O.; Nakai, H.; Vreven, T.;Throssell, K.; Montgomery, Jr., J. A.; Peralta, J. E.; Ogliaro, F.;Bearpark, M. J.; Heyd, J. J.; Brothers, E. N.; Kudin, K. N.; Staroverov,V. N.; Keith, T. A.; Kobayashi, R.; Normand, J.; Raghavachari, K.;Rendell, A. P.; Burant, J. C.; Iyengar, S. S.; Tomasi, J.; Cossi, M.;Millam, J. M.; Klene, M.; Adamo, C.; Cammi, R.; Ochterski, J. W.;Martin, R. L.; Morokuma, K.; Farkas, O.; Foresman, J. B.; Fox, D. J.Gaussian 16 Rev. C.01; Wallingford, CT, **2016**.

Entry for the Table of Contents

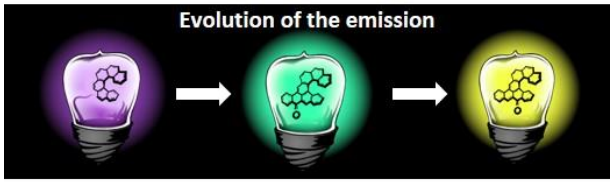

Carbo[n]helicenes are poor emitters with the emission peak in purple or blue region. Inserting a carbonyl group into the skeleton shifts the emission to longer wavelengths and greatly improves the fluorescence quantum yield. The color can be tuned by shifting the position of the carbonyl.